Renewable Energy 39 (2012) 198–206

Contents lists available at ScienceDirect

Renewable Energy

journal homepage: www.elsevier.com/locate/renene

Heat loss of a trapezoidal cavity absorber for a linear Fresnel reflecting solar concentrator

S. Flores Larsen*, M. Altamirano, A. Hernández

INENCO, Instituto de Investigaciones en Energías No Convencionales, Universidad Nacional de Salta, CONICET, Avda, Bolivia 5150, CP 4400, Salta Capital, Argentina

ARTICLE INFO

Article history:
Received 24 February 2011
Accepted 2 August 2011
Available online 23 August 2011

Keywords:
Linear absorber
Fresnel
Trapezoidal cavity
Numerical simulation
Solar thermal

ABSTRACT

The present paper studies the heat loss of a linear absorber with a trapezoidal cavity and a set of pipes used for a linear Fresnel reflecting solar concentrator. The study includes the measurements on a 1.4 m long prototype installed in a laboratory, and its thermal simulation in steady-state using EnergyPlus software. Results of the measured vertical temperature variation inside the cavity, the surface interior and exterior wall and window temperatures, the global heat loss at steady-state and the heat loss coefficients, are presented for six different temperatures of the pipes. Measurements revealed a stable thermal gradient in the upper portion of the cavity and a convective zone below it. Around 91% of the heat transferred to outdoors occurs at the bottom transparent window, for a pipe temperature of 200 °C. The heat loss coefficient per area of absorbing pipes ranged from 3.39 W/m^{2}K to 6.35 W/m^{2}K (for 110 °C $< T_{pipe} <$ 285 °C), and it increased with the increase of T_{pipe}. Simpler and less time-consuming available free software originally designed for heat transfer in buildings was tested to be a possible replacement of the highly complex CFD software commonly used to simulate the steady-state heat loss of the absorber. The experimental and predicted data sets were found to be in good agreement.

1. Introduction

The current world energy situation, with its strong dependence on non-renewable energies and the environmental damage cause by the greenhouse emissions due to fossil fuel burns, calls both, for technology to produce clean energy and for measures to reduce the energy demand. Renewable energies can provide part of the solution, and a great effort is currently made in this field. The generation of electricity by solar thermal energy, by using concentrating systems is a promising technology. One of these concentrating systems is the Linear Fresnel Reflector (LFR), which consists of a mirror array that concentrates solar radiation onto a stationary linear absorber suspended above the array, as shown in Fig. 1. Each mirror is tilted at an angle such that the incident solar rays are reflected to the absorber. The mirrors are installed at ground level and follow the apparent path of the sun by rotating around an axial axis. One or more tubes inside the absorber transport the heat transfer fluid that is heated by the concentrated solar radiation.

The interest on LFRs started around 43 years ago, when Francia [1] studied an LFR installed in Genoa (Italy) in 1963. Since the first oil crisis in 1973, the use of solar concentrators for electricity generation has been experimenting a long and growing evolution. In the second half of the 70's, FMC Corporation in the United States studied an LFR and wrote a detailed report [2]; in the 80's some studies on the performance and concentration characteristics of an LFR were made by Sharma et al. [3], Choudhury and Seghal [4], Mathur et al. [5], and Negi et al. [6]. In the early 90's, Paz Company [7] installed an LFR in Israel, and also in the 90's a system with 300 m^2 of collector area was built in Australia. In 2000, Mills and Morrison [8] developed the Australian compact linear Fresnel reflector (CLFR) concept. Studies and installation of LFR were conducted by Solarmundo group of Belgium and Germany [9]. More recently, the new AUSRA U.S. Company installed LFRs in California [10]. LFR and direct steam generation were also studied in Spain, where solar thermal systems were installed and tested in the South of the country, described in [11–14]. Also in Spain, a concentrating linear Fresnel collector was used in a solar/gas cooling plant at Sevilla [15].

One of the most important roles in an LFR system performance is played by the absorber. Heat loss from the absorber occurs by a complex mechanism that includes radiation, convection and conduction modes. Knowledge of the heat loss through the

* Corresponding author. Tel.: +54 387 4255424; fax: +54 387 4255489.
E-mail addresses: seflores@unsa.edu.ar, silvanafloreslarsen@gmail.com (S. Flores Larsen), martinaltamirano@gmail.com (M. Altamirano), alejo@unsa.edu.ar (A. Hernández).

0960-1481/$ – see front matter © 2011 Elsevier Ltd. All rights reserved.
doi:10.1016/j.renene.2011.08.003

Nomenclature

A_{Mylar}	area of the Mylar film (m^2)
A_{pipes}	total surface area of the absorber pipes (m^2)
A_{top}	area of the exterior side of the absorber top cover (m^2)
h	global convective-radiative heat transfer coefficient (W/m^2K)
h_{Mylar}	convective heat transfer coefficient between the Mylar film and the ambient air (W/m^2K)
k	thermal conductivity of the insulation (W/mK)
L	insulation thickness (m)
Q_d	electric power dissipated by the resistances attached to the pipes (W)
Q_{Mylar}	heat loss from the Mylar film to the outside environment (W)
Q_{top}	heat loss from the top cover surface to outdoors (W)
$T_{ambient}$	ambient air temperature in the laboratory (°C)
T_{floor}	lab floor temperature (°C)
T_{Mylar}	temperature of the Mylar film (°C)
T_{pipe}	average pipe temperature (°C)
$T_{pipe,\ i}$	temperature reached by the pipe i (°C)
$T1-T14$	temperature monitored in the absorber (°C)
U_L	overall heat loss coefficient base on the absorber pipe surface (W/m^2K)
U_{RL}	overall heat loss coefficient based on the receiver length (W/mK)

Greek symbols

ϵ_{Mylar}	infrared emissivity of the Mylar film
σ	Stefan–Boltzmann constant, 5.67×10^{-8} W/m^2K^4

structure surrounding the absorber tubes is very important because it affects the efficiency of the collecting system. The heat loss depends on several factors, as the geometry of the cavity, materials, insulation thickness, infrared emissivity of the absorber surface, concentration ratio, etc. Because of its relevant influence on the system performance, the heat loss of the absorber was subject of research by several methods, including experimental measurements and Computational Fluid Dynamics (CFD) calculations. The inverted cavity was found as the best performing geometry, and the trapezoidal inverted cavity was the preferred geometry of the most recently studied absorbers. Jance et al. [16] demonstrated through heat loss measurements, that convective heat transfer in a trapezoidal cavity is small, and that the heat losses from the cavity are predominantly by radiation. Reynolds et al. [17] and Dey [18] described aspects of the design methodology and the heat transfer calculations for an elevated North–South oriented trapezoidal linear absorber, by using finite element analysis to obtain the absorber temperature distribution, and to optimize the spacing and size of the pipes and the absorber plate (design assumes ducts located above the absorber plate). This study was premised on minimizing the temperature difference between the absorber surface and the fluid inside the ducts and the main conclusion was that sufficiently low temperature differences between the fluid surface and the absorbing surface (<20 K) could be achieved with appropriated spacing and sizes of the pipes, and with practical absorber plate thicknesses. The results are applicable to this particular geometry.

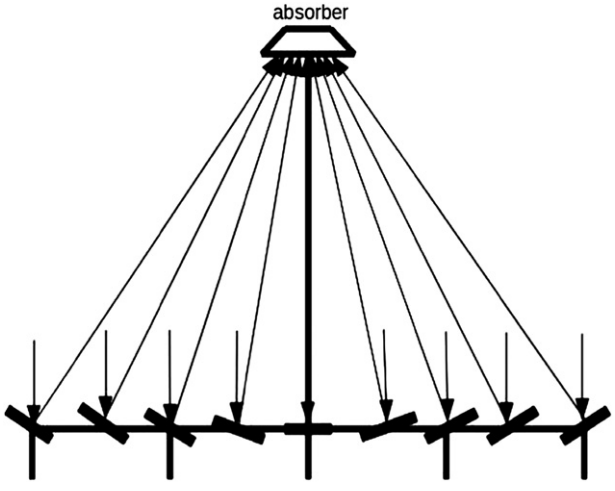

Fig. 1. Schematic representation of a Linear Fresnel Reflector with a trapezoidal absorber cavity.

Reynolds et al. [19] experimentally investigated the heat losses from an absorber with a trapezoidal cross section, with pipes behind the absorber plate. The authors used the flow visualization technique to capture the flow patterns within the cavity and they compared the experimental results with predictions obtained from a model developed with commercial CFD software. The authors achieved excellent agreements between the experimental flow patterns and those predicted by the computational model, but there were differences around 40% between experimentally determined heat losses and those predicted by CFD, which the authors attributed to uncertainties in the experimental work, as the measurement of emissivity and convection and conduction coefficients. The authors also found that the upper two thirds of the cavity is a region of almost zero flow (because the air is stratified due to the hot surface above the air), and that the lower third part of the cavity contains counter-rotating flow cells, one each side of the symmetry plane.

Negi et al. [6] and Khan [20] studied overall heat loss coefficient of concentrically glass covered absorber with non-evacuated tube, coated with ordinary black paint and with oil as fluid flow, reaching temperatures up to 120 °C, and they found poor performances. Singh et al. [21] tested the thermal performance of four identical trapezoidal cavity absorbers with rectangular and round pipe sections. Two absorbing surfaces were compared, one covered with an ordinary dull black board paint and the other consisting of a black nickel selective surface. The experimental data showed that the thermal efficiency of the solar device with round pipe absorber was found higher (up to 8%) as compared to rectangular pipe absorber, that the thermal efficiency decreased with the increase in the concentration ratio of the Fresnel reflecting collector, and that the selective surface coated absorber had a significant advantage in terms of superior thermal performance as compared to ordinary black painted absorber (10% higher). In other very important contribution to the field, Singh et al. [22] studied the steady-state thermal performance of eighth set of identical trapezoidal absorbers with round and rectangular pipes in laboratory conditions, with oil as the pipe fluid. Black ordinary painting and black nickel selective coating with an emissivity of 0.17, obtained by the electroplating process, were tested. Also single and double glass cover (with a glass-to-glass space of 10 mm) were studied, analytically and experimentally. Some important results are that selective coating reduced by 20–30% the overall heat losses of the absorber as compared to ordinary black painting; that double glass cover reduced the overall heat loss coefficient by 10–15% as compared to single glass cover; and that values of the heat loss coefficient of the different cavity absorbers tested in the laboratory lied in the range 3.30–8.2 $W/(m^2\ °C)$.

In Argentina, a group of researchers conducted by Dr. Luis R. Saravia in the Non Conventional Energies Research Institute (INENCO), started the study of linear Fresnel concentrators in 2005. Two prototypes were built and tested, the first one with a mirror area of 8 m^2 [23], and the second one with a mirror area of 24 m^2 [24]. In a new prototype of 42 m^2 recently installed at the INENCO campus, various aspects of the system design were changed, i.e., the previous absorber layout consisting of two pipes of 50 mm in diameter with a compound parabolic concentrator (CPC) mirror as a secondary reflector was changed to 5 pipes of 25 mm in an insulated reflective trapezoidal cavity. Its efficiency was experimentally determined by Salvo et al. [25]. Recent research on LFRs performed at INENCO includes: the computer simulations of the absorber heat transfer by using the electrical–thermal analogy [26]; the simulation of two working options of the Fresnel concentrator, one with direct steam generation and other with recirculating water flow at high pressure in non-stationary state [27]; the applications of LFR for disinfection of substrates [28]; the development of an algorithm to calculate direct solar radiation reflected by an LFR [29]; the study of optical and geometrical aspects of the LFR [30]; and the development of tracking, control and a hail early warning systems [31–33].

The present paper studies the heat loss of a linear absorber with a trapezoidal cavity and a set of pipes used for a linear Fresnel reflecting solar concentrator. The heat transferred at steady-state by conduction, convection and radiation from the fluid-carrying pipes (the absorber) to the outside environment, for different temperatures of the pipes, was determined. The study was carried out by means of indoor measurements on a 1.4 m long absorber prototype, and by thermal simulation in steady-state. As pointed out by Reynolds et al. [19], the interdependence of the three modes of heat transfer, combined with relatively complex geometry and boundary conditions renders the problem difficult to investigate analytically, and so a combination of experimental and computational techniques are needed. The paper presents new results of the measured vertical temperature profile inside the cavity, that confirm the results found by Reynolds et al. [19] through flow visualization and CFD. The interior and exterior surface temperatures of the absorber cover, the window temperature, the global heat loss at steady-state and the heat loss coefficients, are presented. On the other hand, simpler and less time-consuming available free software originally designed to simulate the heat transfer in buildings was tested. This soft was found to be a possible replacement of the complex CFD software commonly used to simulate the absorber heat loss, in cases where a deep knowledge of flow patterns and cavity temperature distributions are not needed.

2. Experimental device

A prototype consisting of a segment of the real collector was built. The trapezoidal cavity is 373 mm deep by 1400 mm in length (Fig. 2). The lower surface of the cavity is 725 mm wide, the upper surface is 220 mm wide, and the angle subtended by the horizontal and lateral wall is 45°. With the exception of length, all other dimensions and materials of the prototype match the real collector geometry and construction. The exterior trapezoidal structure was formed from galvanized sheet metal, with a 120 mm thick insulating material (rock wool) placed around the top and the sides of the cavity, and with a 60 mm thick insulation around the ends, to minimize heat losses. The interior surface of the cavity is a high reflectance polished aluminized sheet. An array of five steel pipes (1.4 m long, 25 mm and 33 mm of interior and exterior diameters, respectively) coated with mate black high temperature painting (emissivity of 0.88) is placed at the top of the trapezoidal cavity. A transparent film sheet (Mylar®, 150 μm) is used in the bottom window. To simulate the heating of the pipes due to absorption of the solar radiation received from the concentrating mirrors, an electrical resistance of 80 Ω (600 W) is installed inside each pipe. The resistances are connected in parallel to a 220 V source, and the power delivered to the absorber was measured by using an AC voltage meter and an AC current clam meter under steady-state. To warm up the pipes to the operating temperatures of interest, a variable resistance is used to reduce the power delivered to the pipes. Fig. 2 shows a photograph taken looking up into the trapezoidal cavity.

The emissivity of the black high temperature painting was previously measured by using an infrared camera FLUKE Model Ti55. A square sample of 30 mm × 30 mm coated with this paint was heated to 290 °C and the emissivity was determined by varying the emissivity value set on the infrared camera until the sample temperature sensed by the equipment equaled the temperature sensed by a calibrated K-thermocouple placed on the sample surface. An average value of 0.88 was obtained.

Surface and air temperatures were measured with K-type calibrated thermocouples connected to a data acquisition system DIGISENSE®. The signals were recorded and stored every 5 min. The monitoring period was set to 6 h, a time duration determined by previous experiments that ensures the achievement of the steady-state in each test. The temperatures showed in the next sections

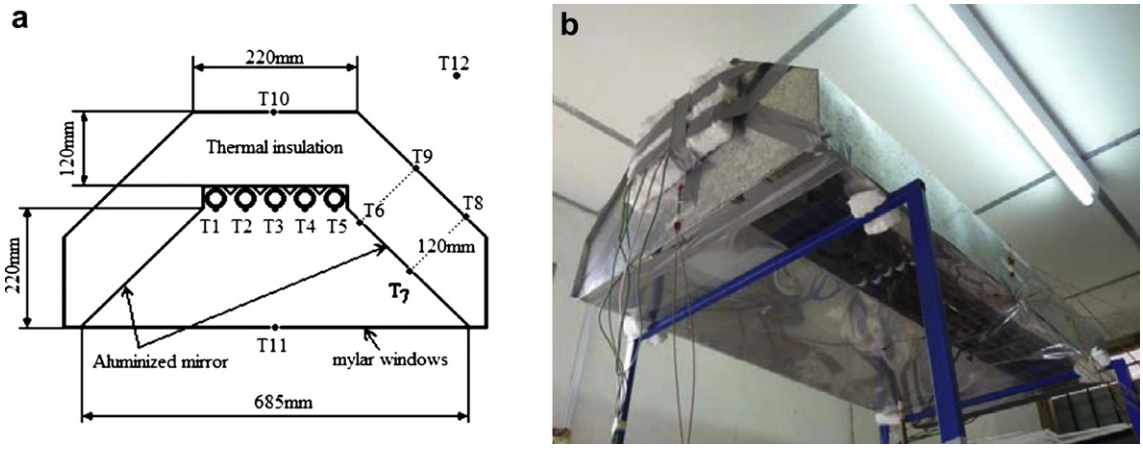

Fig. 2. (a) Cross section of the absorber. (b) Photograph of the prototype in the laboratory.

correspond to the temperatures measured once the steady-state was reached. Twelve thermocouples were installed in the central section of the prototype and in the laboratory, as shown in Fig. 2. $T1-T5$ correspond to the external surface temperatures of the pipes, $T6$ and $T7$ are the temperatures of the interior aluminized surface in two positions (to assess the magnitude of thermal gradients on this surface because the air is warmer next to the pipes and cooler near the Mylar® cover), $T8$ and $T9$ correspond to the temperature of the outside galvanized sheet metal cover at points in front of $T7$ and $T6$ respectively (perpendicular to the cover surface, in order to evaluate the thermal gradient through the insulation), $T10$ corresponds to the exterior surface temperature of the top cover that is measured to evaluate the thermal gradient through the insulation in the hottest sector of the prototype, $T11$ is the temperature of the Mylar® film, and finally $T12$ is the room air temperature at a point halfway up in the laboratory. $T13$ and $T14$ are the outer and inner surface temperatures of one of the absorber ends (not shown in the absorber section of Fig. 2) and they were sensed by a digital thermometer DIGISENSE®. The same instrument was used to sense the floor temperature under the prototype, to account for the radiative heat transfer between the floor and the Mylar cover. In order to determine the temperature profile inside the cavity, the air temperature was registered with a manual thermometer DIGISENSE® at eleven points along the vertical axis of the prototype, spaced 20 mm from each other, from the Mylar® cover to the pipes.

3. Monitoring results

The absorber pipes were heated to reach different temperatures covering an interval that ranged from 110.7 to 284.8 °C. In each one of the 6 tests conducted in the laboratory, the electric power Q_d (W) dissipated by the resistances attached to the pipes was registered at steady-state. These values are a direct measure of the heat dissipated by the absorber to the surroundings at steady-state. The results are presented in Table 1, Figs. 3 and 4.

Table 1 shows the values of the delivered electrical power (Q_d), the ambient air temperature in the laboratory ($T_{ambient}$), the lab floor temperature (T_{floor}), the temperatures reached by each pipe ($T_{pipe,\ i}$), and the mean pipe temperature obtained from averaging the individual temperatures of the pipes (T_{pipe}). The heat loss ranged from 180 W to 1130 W, with average pipe temperatures between 110.7 °C and 284.8 °C. Fig. 3a shows the surface temperature achieved by the 5 pipes, where a spatial symmetry with respect to the central pipe is observed in all tests. The average difference between the maximum temperature achieved in the central pipe and the temperature of the lateral pipe is 8.8%. As it was not possible to guarantee that each resistor dissipate exactly the same power, it is risky to assert that the central hottest pipe had the lowest net loss of heat due to its privileged position within the array of tubes. It is noted, besides, that the temperatures of the two end pipes (1 and 5) are slightly different, which could arise from slightly differences in the power dissipated by the resistors and/or from small differences in the R-values of the side walls.

Table 1
Steady-state delivered electrical power (Q_d), ambient air temperature in the laboratory ($T_{ambient}$), lab floor temperature (T_{floor}), temperatures reached by the pipes ($T_{pipe,\ i}$), and mean pipe temperature obtained from averaging the individual temperatures of the pipes (T_{pipe}).

N° test	Q_d (W)	$T_{ambient}$ (°C)	T_{floor} (°C)	$T_{pipe,\ 1}$ (°C)	$T_{pipe,\ 2}$ (°C)	$T_{pipe,\ 3}$ (°C)	$T_{pipe,\ 4}$ (°C)	$T_{pipe,\ 5}$ (°C)	T_{pipe} (°C)
1	1130	40.2	31.8	281.8	284.5	290.0	287.3	280.3	284.8
2	825	30.3	23.6	234.1	238.9	248.2	238.3	228.2	237.5
3	580	27.6	22.7	195.6	199.6	207.3	199.1	190.9	198.5
4	430	29.7	20.7	169.7	173.3	179.9	172.9	165.1	172.2
5	360	25.6	20.0	153.7	157.1	162.9	156.5	149.7	156.0
6	180	37.8	28.9	108.7	111.3	115.0	111.9	106.5	110.7

Fig. 3b shows the measured vertical temperature profile of the air inside the cavity for each test. The difference between bottom and upper air temperature grows with the delivered power, from 36.1 °C (for 180 W) to 57.8 °C (for 1130 W). The obtained temperature profiles indicate that there are three regions defined inside the cavity. As expected, in the upper region the air presents a thermal gradient, indicating that the air is stably stratified due to the hot surface above the air. In this region, the thermal gradient is stronger as greater is the power dissipation, that is, the greater the surface temperature of the pipes. In the middle zone between 40 and 100 mm from the bottom window, the thermal gradient is weaker, possibly due to the existence of a convective zone. In the bottom zone, below 40 mm, there is only one measurement point, at 20 mm, so it is no possible to infer any flow regime, but it is clear that in this zone the temperature is lower than in the convective zone for all tests. The measured profile, with an upper stratified zone and a convective zone, is in line with Reynolds et al. [19], who predicted by CFD and experimentally confirmed the existence of a stratified profile in the upper two thirds of the cavity, and counter-rotating flow cells, one each side of the symmetry plane, in the lower third part of the cavity. However, the geometric dimensions of the cavity tested by Reynolds are slightly different to the dimensions of the absorber presented in this paper, which could explain the differences found in the experiments.

Fig. 4 shows the measured temperatures of the interior and exterior surfaces of the prototype, and the Mylar® temperature. The temperatures were plotted against the average pipe temperature reached in each test. Temperatures sensed at inside surfaces were plotted with diamonds, while temperatures sensed on the outer shell were plotted with triangles. Both, interior and exterior surface temperatures increase with the average temperature of pipes, as expected for the steady-state response of a lightweight thermally insulated cavity with internal heat generation.

The difference observed in the internal temperatures of the side walls at an upper and a lower position ($T6$ and $T7$), grows from around 11.5 °C (for pipe temperatures of 110.6 °C) to 43.7 °C (for a pipe temperature of 284.8 °C). This difference indicates that the temperatures of the lateral sides are not uniform, and that there is an upward thermal gradient on the surface of polished aluminum caused by the heat conduction through the metal sheet, from the upper cover where the pipes are attached to the lateral sides, reinforced by the air temperature distribution inside the cavity, which grows upwards too. Because the differences are significant for high pipe temperatures, it could be a reasonable option to break the thermal bridge between the upper and the lateral covers, in order to lower the lateral temperatures and, as a consequence, the thermal losses. The interior temperature of the end cover ($T14$) was measured at a point that is at an intermediate level between $T6$ and $T7$, hence its value is between those of them. Since the temperature of the Mylar® film is higher than the air layer that is on it (see Fig. 3b), the heating of the Mylar® comes exclusively from the infrared radiative exchange with the pipes and the lateral aluminized surfaces.

There are not great differences between the temperatures at different points in the outer shell, that is, between the lateral side temperatures ($T8$ and $T9$) and the absorber roof temperature ($T10$). The exception is the temperatures of the end cap ($T13$), which is higher than the previous one because the thickness of the insulation in this area is half the thickness of the rest of the prototype.

The heat loss Q_{Mylar} (W) from the Mylar film to the outside environment can be estimated by:

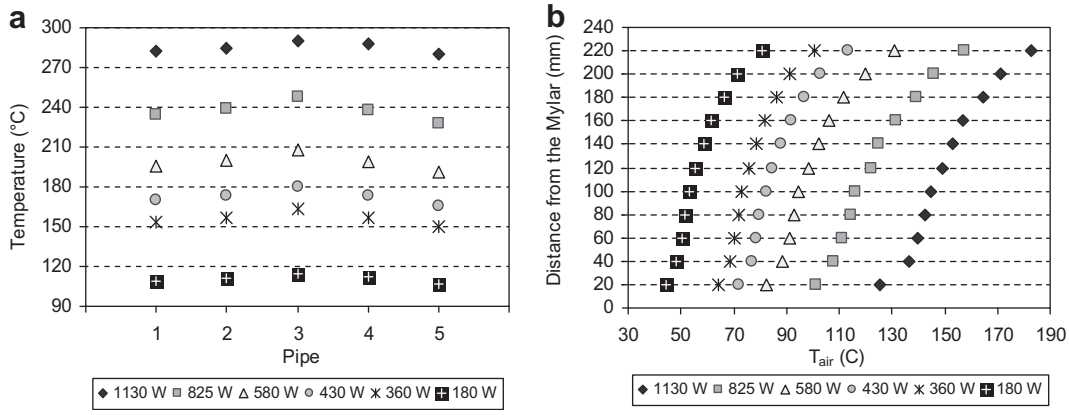

Fig. 3. a) Measured surface temperature of the pipes for each test. b) Vertical air temperature profile inside the cavity at different distances from the bottom window, for each test.

$$Q_{\text{Mylar}} = A_{\text{Mylar}} h_{\text{Mylar}} \left(T_{\text{Mylar}} - T_{\text{ambient}}\right) + \sigma \varepsilon_{\text{Mylar}} A_{\text{Mylar}} \left(T^4_{\text{Mylar}} - T^4_{\text{floor}}\right) \quad (1)$$

where A_{Mylar}, $\varepsilon_{\text{Mylar}}$, T_{Mylar} are the area, infrared emissivity and temperature of the Mylar film, T_{floor} is the floor surface temperature, σ is the Stefan–Boltzmann constant, T_{ambient} is the air ambient temperature, and h_{Mylar} is the convective heat transfer coefficient between the Mylar surface and the ambient air. Because the absorber was tested in a laboratory without forced air movement, we assumed low air velocities and low outside convective heat transfer coefficient (0.96 W/m^{2}K), taken for a horizontal surface with reduced convection [34]. In an absorber placed outside, this value will be greater because it depends on wind velocity. Thus, for a power dissipation of 580 W (from Table 1: $T_{\text{pipe}} = 198.5$ °C, $T_{\text{Mylar}} = 95$ °C, $T_{\text{ambient}} = 27.6$ °C, $T_{\text{floor}} = 22.7$ °C, $A_{\text{Mylar}} = 0.96$ m^2, $h_{\text{Mylar}} = 0.96$ W/m^{2}K), the thermal loss of the Mylar estimated from Eq. (1) is around 530 W from which 470 W (88%) is lost by radiation. This means that around a 91% of the absorber heat loss occurs at the Mylar film. This result agrees with those found by Reynolds et al. [19] and it is similar to the value of 87% that was estimated analytically from a global energy balance at stationary state described in [35].

In Fig. 5a Q_d vs $(T_{\text{pipe}} - T_{\text{ambient}})$ was plotted. The experimental values were fitted by a power curve:

$$Q_d = 0.245\left(T_{\text{pipe}} - T_{\text{ambient}}\right)^{1.5184} \quad (\text{W}); R^2 = 0.98 \quad (2)$$

This expression is valid in the range 110 °C < T_{pipe} < 285 °C.

The overall heat loss coefficient U_L in W/m^{2}K referred to the absorber area was calculated from:

$$U_L = \frac{Q_d}{A_{\text{pipes}}\left(T_{\text{pipe}} - T_{\text{ambient}}\right)} \quad \left(\frac{\text{W}}{\text{m}^2\text{K}}\right) \quad (3)$$

where A_{pipes} is total surface area of the absorber pipes (0.73 m^2 for the tested prototype). In Fig. 5b, the heat loss coefficient U_L estimated through Eq. (3) was plotted against the difference on the pipe temperature and the outside air temperature. The obtained values ranged from 3.39 W/m^{2}K to 6.35 W/m^{2}K, that are in the range of other values found in the literature. Singh et al. [22] found experimental values of the overall heat loss coefficient ranging from 4.6 to 7.31 W/(m^{2}K) (for T_{pipe} between 75 °C and 175 °C). These values correspond to a trapezoidal cavity absorber of 2170 mm length, with six round pipes of 16 mm outer diameter, coated with black ordinary painting, single glass cover, an angle of around 33° between lateral cover and glass, and glass wool insulation (100 mm thick) at the upper portion and sides of the absorber pipes.

The best-fit curve between heat loss coefficient and absorber temperature followed a power curve pattern which was in line with Singh et al. [21,22], Khan [20] and Negi et al. [6], who assess that the power curve may be attributed to the dominance of radiation losses, which increases significantly with temperature. The fitted curve is then given by

$$U_L = 0.357\left(T_{\text{pipe}} - T_{\text{ambient}}\right)^{0.5184} \left(\frac{\text{W}}{\text{m}^2\text{K}}\right); R^2 = 0.89 \quad (4)$$

This expression is also valid in the range 110 °C < T_{pipe} < 285 °C and it is close to the expression found by Singh et al. [22] ($U_L = 0.3521(T_{\text{pipe}})^{0.6076}$ W/m^{2}K) for the single glass cover cavity described before.

It is common to find in the literature the global heat transfer coefficient based on the receiver length, the mirror area, the aperture area, etc. To compare the measured data with other available data, expression (4) can be modified to give a global heat transfer coefficient U_{RL} based on the receiver length, that is:

$$U_{\text{RL}} = 0.186\left(T_{\text{pipe}} - T_{\text{ambient}}\right)^{0.5184} \left(\frac{\text{W}}{\text{mK}}\right); \quad 110^{\circ}\text{C} < T_{\text{pipe}} < 285^{\circ}\text{C} \quad (5)$$

This correlation gives heat transfer coefficients which are comparable to the values found in the literature for different types of linear absorbers. I.e., for $T_{\text{pipe}} - T_{\text{ambient}} = 200$ °C, Eq. (5) gives a heat transfer coefficient of 2.9 W/mK. Other studies of absorbers with non-evacuated tubes found in the literature give values of

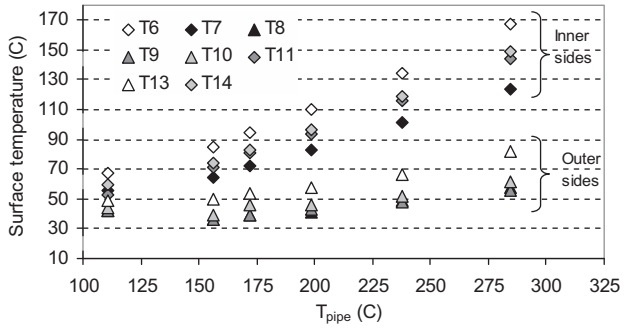

Fig. 4. Measured temperatures on the absorber surfaces at steady-state, for different average pipe temperatures.

2.0 W/mK [36], 1.25 W/mK [37], and 1.0 W/mK [38]. It is important to note that the mentioned absorbers have significant differences between them, i.e., the number of tubes, the geometry, the infrared emittance due to the selective paintings, use of CPC cavities, etc., and it explains the variations in the values of the overall heat loss coefficients. The geometry and materials of the absorber reported in this paper is more similar to that reported by Singh et al. [21,22].

4. Thermal simulation of the absorber

The steady-state thermal behavior of the absorber was simulated with EnergyPlus v5.0 for Windows [39]. Originally, this software was developed by NREL to simulate the transient thermal behavior of multizone buildings. The thermal models included in the software are suitable for the simulation of a solar system like a linear Fresnel absorber, by considering that the cavity itself is a thermal zone connected with outdoors through elements conveniently defined at the data input stage. Thus, the advantages of EnergyPlus in calculation, thermal modeling and presentation of results can be profited to simulate the temperatures inside the cavity (air and surface temperatures), and to estimate the global heat losses for different pipe temperatures.

EnergyPlus models include the infrared heat exchange between surfaces, that is, between outside surfaces and the surroundings, and between surfaces inside the zone. The air in the zone is assumed to be completely transparent to infrared radiation, and the ScriptF model developed by Hottel [40] is used, which assumes a gray interchange model for the longwave radiation. The thermal emissivities of all surfaces must be defined by the user, as well as the infrared transmittance at normal incidence for transparent surfaces.

4.1. Description of the absorber in EnergyPlus

The actual absorber geometry was simplified as shown in Fig. 6. An absorber 1400 mm long and 390 mm high, with a bottom window aperture of 715 × 1400 mm, was simulated. The absorber elements connecting the air in the cavity with outdoors are: four lateral insulated covers, the bottom transparent window, and the top cover with the hot pipes.

The following assumptions were made:

- Steady-state
- The trapezoidal cavity was considered a unique thermal zone with homogeneous air temperature.
- The tubes are replaced by a plane surface of known temperature.
- The cavity cover has negligible thermal mass, and it is described by its thermal resistance.

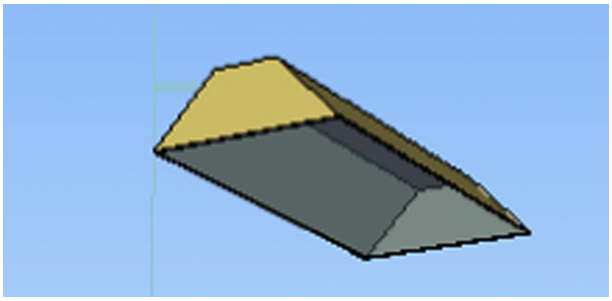

Fig. 6. Schematic of the absorber cavity showing the unique thermal zone defined in EnergyPlus.

- The conduction heat transfer is one dimensional.
- Each surface of the absorber has a uniform temperature distribution. The temperatures of interior and exterior sides of lateral, top, and bottom surfaces are calculated by the soft and all heat transfer modes (conduction, convection and infrared radiation) are included.
- A unique known external air temperature was used.
- Constant external and internal convection coefficients were used, with different values for each surface in the absorber.
- Heating of the transparent glazing due to the absorption of infrared radiation was accounted for.

The assumed hypotheses realized the fact that radiation exchange (the most significant heat transfer mode in the absorber) was modeled in detail in EnergyPlus, and that internal convection is not treated with such detailed level. Measurements indicate that there are convective cells inside the cavity and a stratified zone and the calculation of such air movement profiles cannot be modeled without CFD (needing as inputs the boundary conditions supposed for each surface, which are not always available). A possible simplified way to deal with this subject that was adopted in this research, is to consider constant *h*-values for each surface and to test if the supposed values can predict the experimental data. Thus, internal and external convective coefficients were estimated by using the *Simple* and *Detailed Natural Convection algorithms* provided by EnergyPlus and they were entered as constant values for all simulations. External convective coefficient of 1.6 W/m^{2}K was used for lateral covers, while values of 0.96 W/m^{2}K were used for hot horizontal surfaces (outside Mylar® surface and inside black surface) corresponding to the convective coefficient on a horizontal surface with reduced convection due to air stratification. Internal convective coefficients were 4.04 W/m^{2}K for the internal side of the transparent glazing

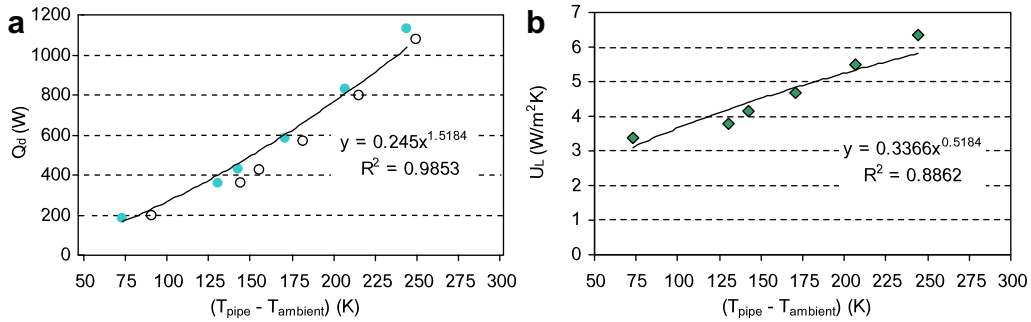

Fig. 5. (a) Power dissipation Q_d versus the difference between the average pipe temperature and the outside ambient air. (b) Heat loss coefficient U_L calculated from Eq. (4) versus the difference between the average pipe temperature and the outside ambient air.

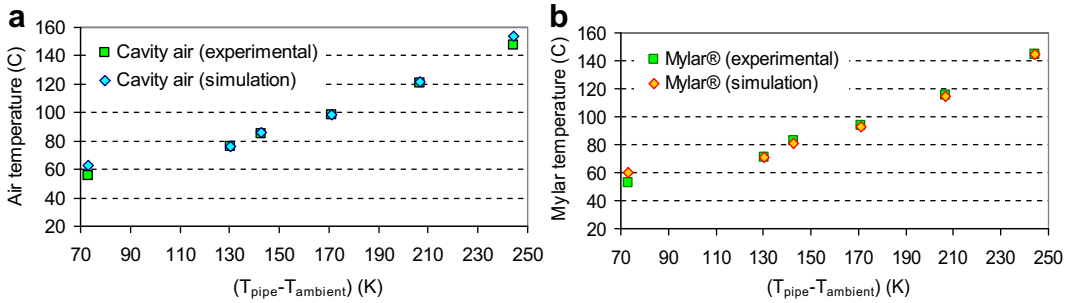

Fig. 7. (a) Experimental and simulated temperatures of the air in the absorber cavity; (b) Experimental and simulated temperatures of the transparent Mylar® film.

(horizontal surface with enhanced convection), and 1.2 W/m^{2}K for the other internal cover surfaces.

Six temperatures of the top hot surface were simulated, corresponding to average pipes temperature obtained in the experiments: 110, 156, 172, 199, 238, and 285 °C. EnergyPlus allows the managing of the outside boundary conditions of the elements, i.e., it allow to fix the surface temperature of the exterior side of an element (but not the temperature of an interior side). The adopted solution was to consider that the exterior side of the top cover of area A_{top} is at the desired temperature T_{pipe} and to define this cover as a thin metal sheet, thus its high conductivity ensures an interior temperature equal to the exterior one. The heat loss Q_{top} from this surface to outdoors was estimated separately by using a global convective–conductive heat transfer coefficient (thus, $Q_{top} = A_{top}(T_{pipe} - T_{ambient})/(L/k + 1/h)$, with L the insulation thickness, k the thermal conductivity of the insulation, and h the convective-radiative heat transfer coefficient) and it was added to the global heat loss obtained by the software.

Thermal resistance of the cover was fixed, at 2.0 m^{2}K/W, an average value that includes the effect of the lower thickness of insulation in the bottom part of the lateral covers. The thermal conductivity of the transparent Mylar® film is 0.5 W/mK. The emissivity value of 0.88 for the absorber surface (black non-selective painting) was obtained from measurements, as it was explained in the previous section. Because radiation is the dominant mode of heat transfer, the accuracy of the absorber surface emissivity value is critical to successfully model the heat transfer in the cavity. Hemispherical infrared emissivity of internal aluminized surface was taken as 0.1, while 0.88 was used for the Mylar® film [41]. Because the experiments simulated the absorption of solar radiation by heating the pipes at the top surface, optical properties of materials in the solar and visible spectrum are not used by the software and there is no need of accuracy for these values.

The weather file managed by EnergyPlus contains hourly values of the outdoor variables needed to perform the simulation. These values were changed in the file to agree with the experimental values, i.e., outdoor air temperature was replaced by the air temperature measured in the laboratory during each experiment. Solar radiation data remained unchanged because the absorber was simulated in an indoor environment and exterior surfaces were defined with a “No Sun Exposure” label.

4.2. Results of the simulations

The results of the simulations are shown in Figs. 7 and 8 for the temperatures of the air in the cavity, the surface temperatures of Mylar®, the surface temperatures of the lateral covers (internal and external sides), and the absorber global heat loss. To compare the simulated temperatures of the air in the cavity with measured data, a weighted average of the data obtained in the experimental profile was made to obtain a single value for each test. Interior surface temperatures of the four lateral covers were averaged to obtain a representative value of the interior surface temperature. The same procedure was used to obtain the exterior surface temperature of the lateral cover. A good agreement between simulated and experimental data was found for all series. For high temperatures, experimental and simulated temperatures for cavity air and lateral cover surfaces have a little difference (Figs. 7a and 8a), because the actual convective heat transfer coefficient is larger than the average value used in the model, but we consider that using a unique value for all simulations does not account for severe errors, particularly in the estimation of the absorber heat losses. In Fig. 8b, the average percent error between predicted heat losses and the actual values is 6.5%. As shown, the software gives accurate results for temperatures of the air cavity, for the inside and outside surfaces, and for the global heat loss.

In Fig. 9, the heat loss coefficient per area of absorbing pipes (U_L) was plotted versus the difference between the average pipe temperature and ambient lab temperature, for pipes coated with ordinary black painting and with selective black painting. As

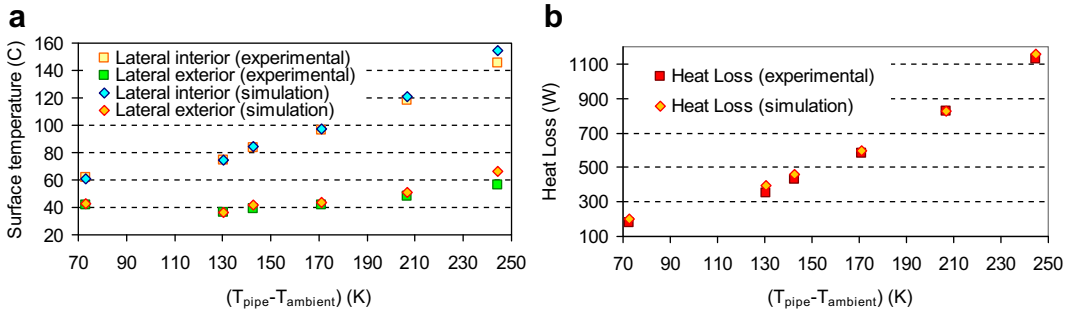

Fig. 8. (a) Experimental and simulated temperatures of the lateral surfaces of the absorber cover; (b) Experimental and simulated absorber heat loss.

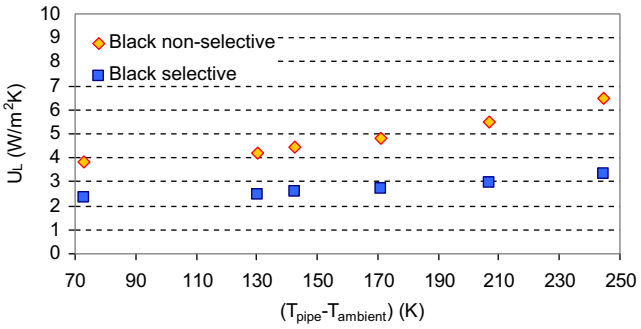

Fig. 9. Simulated heat loss coefficient per area of absorbing pipes (U_L) versus the difference between the average pipe temperature and ambient lab temperature, for pipes coated with non-selective and selective black painting.

expected, the heat loss coefficient U_L increases as the difference ($T_{pipe} - T_{ambient}$) increases. The values of the heat loss coefficient for ordinary black painted and selective surface coated absorbers lies in the range of 5.32–9.11 and 3.31–4.66 W/km^2, respectively. The use of the selective coating on the surface of the pipes results in a considerable decrease of the heat loss coefficient which is desirable. Reductions between 38% and 49% in the heat transfer coefficient are obtained when a selective black painting is used, with higher reductions for higher temperatures of the pipes. The higher values of U_L when non-selective coating is used can be attributed to the higher radiation heat losses of the ordinary black coating (emissivity at 290 °C = 0.88) as compared to a commercial selective coating (emissivity at 400 °C = 0.27, [42]).

The results show that the heat transfer models included in EnergyPlus were easily adapted to study the thermal behavior of the absorber in steady-state. The use of a unique thermal zone and constant convective heat transfer coefficients implies an extremely quick and simple data input stage. The use of constant convective coefficients is supported by the research of Reynolds et al. [19], who conducted a sensitivity analysis using a CFD computational model and concluded that the convection coefficients applied to the walls and window have negligible effect on the power consumption of the heaters, when compared with effects due to the emissivity of the heater surface, over a large range of values.

5. Conclusions

The steady-state thermal behavior of an LFR absorber prototype was studied. The power dissipated by electric resistances installed inside the absorber pipes was varied in order to obtain different surface temperatures in the range between 110 °C < T_{pipe} < 285 °C, which is the range of operation temperatures of a real absorber. The tests were performed in a laboratory without artificial air conditioning or forced air movement.

The results obtained during the thermal monitoring of the prototype were evaluated, and the heat loss coefficient versus the difference between the pipes and the outside environment temperatures, was found. The obtained values ranged from 3.39 to 6.35 W/m^{2}K, and they increased with the increase of T_{pipe}. An analytical expression for this coefficient was obtained that follows a power curve. This expression is useful for determining the absorber efficiency in the working range 110 °C < T_{pipe} < 285 °C. Measurements of the air temperature taken at different heights between the Mylar cover and the pipes revealed the existence of a stable thermal gradient in the upper portion of the cavity and a convective zone between 40 mm and 100 mm from the bottom surface. Because the temperatures recorded on the transparent cover are consistently higher than those of the air registered at 20 mm of the film, it is concluded that further measurements are needed, especially at the region between 0 and 60 mm.

The calculated thermal behavior of the absorber by using the thermal model of EnergyPlus resulted in good agreement with the experimental data. Such a thermal model can be used to optimize the thermal efficiency of the absorber, by testing different environmental conditions, changing materials, geometry, etc., without the need of building and testing new prototypes. Future research with EnergyPlus will include the simulation of the absorber in outdoor environments. In this case, the parabolic shape of the Fresnel linear mirrors can be modeled in EnergyPlus as a group of reflective plane surfaces forming the parabolas that collect the solar energy and redirect it to the absorber window.

Finally, an important conclusion that was obtained from the experimental data, is that the highest portion of the thermal loss occurs by radiation from the window surface, i.e., for a pipe temperature around 200 °C around 91% of the heat is lost from the bottom window. This fact should be considered in order to improve the thermal efficiency of future designs.

Acknowledgments

This research was supported by Universidad Nacional de Salta, ANPCYT PICTO 32140 and PICTO ENARGAS 2009-0192.

References

[1] Francia G. Pilot plants of solar steam generating stations. Solar Energy 1968; 12:51–64.
[2] Di Canio, G., Treytl, W.J., Jur, F.A., Watson, C.D., 1979. Line focus solar thermal central receiver research study––final report. Prepared for the US Department of Energy by FMC Corporation, Santa Clara, CA, DOE/ET/20426–1, April 1979.
[3] Sharma MS, Mathur SS, Singh RN. Performance analysis of a linear solar concentrator under different flow regimes. Applied Energy 1983;13(1):77–81.
[4] Choudhury C, Sehgal HK. A Fresnel strip reflector–concentrator for tubular solar-energy collectors. Applied Energy 1986;23(2):143–54.
[5] Mathur SS, Kandpal TC, Negi BS. Study of concentration characteristics and performance evaluation of a linear Fresnel reflector. In: Proc. of National Solar Energy Conv. New Delhi: Tata McGraw Hill Publishing Co; 1988. p. 263–70.
[6] Negi BS, Mathur SS, Kandpal TC. Optical and thermal performance evaluation of a linear Fresnel reflector solar concentrator. Solar Wind Technology 1989; 6(5):589–93.
[7] Feuermann, D., Experimental evaluation of the PAZ. Solar thermal collector at the Ben-Gurion centre for solar thermal electricity generating technologies. Final report, Prepared for the Ministry of Energy and Infrastructure, State of Israel. 1993.
[8] Mills DR, Morrison GL. Compact linear Fresnel solar thermal power plants. Solar Energy 2000;68(3):263–83.
[9] Haberle A, Zahler C, de Lalaing J, Ven J, Sureda M, Graf W, et al. The Solarmundo project: advanced technology for solar thermal power generation. Adelaide, Australia. In: Proceedings of the ISES 2001 Solar World Congress; 2001. 25–30 November.
[10] AUSRA, 2010. http://www.ausra.com [accessed 02.11].
[11] Zarza E, Rojas ME, González L, Caballero JM, Rueda F. INDITEP: the first pre-commercial DSG solar power plant. Solar Energy 2006;80(10):1270–6.
[12] Zarza E. Personal communication. PSA, 2007. Plataforma Solar de Almería, http://www.psa.es; 2007.
[13] Eck M, Bahl C, Bartling KH, Biezma A, Eickhoff M, Ezquierro E, et al. Direct steam generation in parabolic trough at 500 °C – A German–Spanish project targeted on component development and system design. In: Proc. Of 14th international solar PACES symposium on solar thermal concentrating technologies; 2008. Las Vegas, USA.
[14] Montes MJ, Abánades A, Martínez-Val JM. Performance of a direct steam generation solar thermal power plant for electricity production as a function of the solar multiple. Solar Energy 2009;83(5):679–89.
[15] Bermejo P, Pino FJ, Rosa F. Solar absorption cooling plant in Seville. Solar Energy 2010;84:1503–12.
[16] Jance MJ, Morrison GL, Behnia M. Natural convection and radiation within an enclosed inverted absorber cavity: preliminary experimental results. In: Renewable energy transforming business: proceedings of solar. Brisbane: ANZSES; 2000. 29 November–1 December 2000.
[17] Reynolds DJ, Behnia M, Morrison GL. Heat transfer in a trapezoidal cavity for a solar thermal collector. In: Renewable energy transforming business proceedings of solar 2000. Brisbane: ANZSES; 2000. 29 November–1 December 2000.

[18] Dey C. Heat transfer aspects of an elevated linear absorber. Solar Energy 2004; 76:243–9.
[19] Reynolds D, Jance MJ, Behnia M, Morrison GL. An experimental and computational study of the heat loss characteristics of a trapezoidal cavity absorber. Solar Energy 2004;76:229–34.
[20] Khan Md KA. Copper oxide coating for use in a linear solar Fresnel reflecting concentrating collector. Renewable Energy 1999;7:603–8.
[21] Singh PL, Sarviya RM, Bhagoria JL. Thermal performance of linear Fresnel reflecting solar concentrator with trapezoidal cavity absorbers. Applied Energy 2010;87:541–50.
[22] Singh PL, Sarviya RM, Bhagoria JL. Heat loss study of trapezoidal cavity absorbers for linear solar concentrating collector. Energy Conversion and Management 2010;51:329–37.
[23] Gea M, Saravia L, Fernández C, Caso R, Echazú R. Concentrador lineal Fresnel para la generación directa de vapor de agua. Avances en Energías Renovables y Medio Ambiente 2007;11:03.83–9.
[24] Saravia L, Gea M, Fernández C, Caso R, Hoyos D, Salvo N, et al. Diseño y construcción de un concentrador lineal de Fresnel de 24m^2 de área. Avances en Energías Renovables y Medio Ambiente 2008;12:03.119–24.
[25] Salvo N, Altamirano M, Bárcena H, Saravia L. Ensayo de un concentrador Fresnel. Cálculo de eficiencia. Avances en Energías Renovables y Medio Ambiente 2009;13:03.99–03.104.
[26] Altamirano M, Flores Larsen S, Hernández A, Saravia L. Simulación térmica de un absorbedor lineal mediante SIMUSOL. Avances en Energías Renovables y Medio Ambiente 2009;13:03.25–30.
[27] Altamirano M, Gea M, Placco C, Saravia L, Alía D. Simulación térmica de un concentrador lineal tipo Fresnel, dos opciones de funcionamiento. Avances en Energías Renovables y Medio Ambiente 2010;14:03.139–46.
[28] Placco C, Saravia L, Gea M, Altamirano M, Fernández C, Herrando C. Desinfección de sustrato con vapor utilizando un concentrador Fresnel lineal. Avances en Energías Renovables y Medio Ambiente 2010;14:03.207–13.
[29] Salazar G, Cadena C. Algoritmo para el cálculo de ángulos de radiación solar directa, incidente y reflejada, en un sistema de concentradores Fresnel simplificado. Avances en Energías Renovables y Medio Ambiente 2009;13:03.139–46.
[30] Gea M, Saravia L, Altamirano M, Placco C, Bárcena H, Hongn M. Aspectos ópticos geométricos de un concentrador solar Fresnel lineal para aplicaciones térmicas. Avances en Energías Renovables y Medio Ambiente 2010;14:03. 215–22.
[31] Salazar G, Cadena C. Sistemas informáticos para el diseño, control y alerta en un sistema concentrador tipo Fresnel. Avances en Energías Renovables y Medio Ambiente 2010;14:08.107–11.
[32] Cadena C, Echazú R. Sistema de enfoque y seguimiento para espejos planos de gran longitud. Avances en Energías Renovables y Medio Ambiente 2009;13: 08.169–74.
[33] Hoyos D, Serrano V, Villena M, Moya T, Goglino J. Sistema de control para generadores de vapor utilizando concentradores solares tipo Fresnel. Avances en Energías Renovables y Medio Ambiente 2010;14:08.143–50.
[34] EnergyPlus Documentation, Engineering Reference, pp.77, taken from ASHRAE Handbook, 1985.
[35] Altamirano M, Hernández A, Flores Larsen S, Saravia L. Evaluación experimental de las pérdidas térmicas en el absorbedor de un concentrador lineal tipo Fresnel. Avances en Energías Renovables y Medio Ambiente 2009;13:03. 17–24.
[36] Häberle A, Zahler C, Lerchenmüller H, Mertins M, Wittwer C, Trieb F, et al. The Solarmundo line focussing Fresnel collector. Optical and thermal performance and cost calculations. Zürich. In: International symposium on concentrated solar power and chemical energy technologies; 2002.
[37] Feuermann D, Gordon JM. Analysis of a two-stage linear Fresnel reflector solar concentrator. Journal of Solar Energy Engineering, Transactions of the ASME November 1991;113:272–9.
[38] Facão J, Oliveira A. Numerical simulation of a trapezoidal cavity receiver for a linear Fresnel solar collector concentrator. Renewable Energy 2011;36(1): 90–6.
[39] EnergyPlus. apps1.eere.energy.gov/buildings/energyplus/ [accessed 02.11].
[40] Hottel HC, Sarofim AF. Radiative transfer. New York: McGrawHill; 1967.
[41] Mylar, 2011. http://usa.dupontteijinfilms.com [accessed 02.02.11].
[42] Morales A., Zarza E. (2011). http://www.solec.org/solkotehome.htm [accessed 02.02.11].